APPENDIX B

Late Quaternary Faulting on the Eastgate and Clan Alpine Faults, Nevada

Anthony J. Crone and Michael N. Machette
U.S. Geological Survey
Golden, Colorado

Friends of the Pleistocene, Pacific Cell, Field Trip Stop Description
September 2009

Late Quaternary Faulting on the Eastgate and Clan Alpine Faults, Nevada

Anthony J. Crone and Michael N. Machette
U.S. Geological Survey
Golden, Colorado

Introduction

In the past 137 years, 11 large (M>6.5) historical earthquakes have formed surface ruptures in the Basin-and-Range Province (BRP) of the Intermountain West (de Polo and others, 1991). Six of these historic earthquakes occurred in the north-south-trending Central Nevada Seismic Belt (CNSB; Wallace, 1984), which occupies only a small portion of the BRP. The results of numerous recent paleoseismic studies in the CNSB have shown this cluster of historical earthquakes is anomalous in that a similar sequence of temporally clustered faulting has not been documented during late Quaternary (since 130 ka) time (Bell and others, 2004). Although the slip rates on individual faults in the CNSB, and in the BRP as a whole, are low compared to the slip rates on province-bounding faults associated with the transpressional plate boundary in California, these comparatively low-slip Basin-and-Range faults do pose a significant seismic hazard in urbanized areas such as the Wasatch Front of Utah and the eastern side of the Sierra Nevada Mountains in western Nevada and eastern California (Truckee-Reno and Las Vegas metropolitan areas), both of which are among the more rapidly growing urban areas in the country.

The concentration of historical surface-faulting earthquakes in the CNSB is striking and anomalous when considering the size of the CNSB with respect to the entire BRP (Wallace, 1984; Machette, 2005). This temporal clustering in the CNSB raises fundamental questions about fault mechanics and their interactions, the distribution, accumulation, and release of extensional strain in the crust, as well as the temporal and spatial patterns of paleoearthquakes in the BRP and the CNSB.

Recent geodetic studies in this region indicate about 10–11 mm of WNW-directed extension is occurring in selected belts (presumed to be active fault zones) in the BRP (Bennett, and others, 1998, 2003; Thatcher and others, 1999; Hammond and Thatcher, 2004), yet there are few quantitative data to define exactly how this slip is accommodated on specific faults and whether those faults are releasing strain over geologically significant time scales. The geodetic data provide a contemporary snapshot of strain accumulation, but it remains unknown if the contemporary accumulation directly relates to pending fault failure and thus to the seismic hazard. A geologically based perspective of the long-term (thousands to tens of thousands of years) distribution of surface-rupturing earthquakes offers insights into seismic hazard and crustal-scale strain accumulation processes that complement the short-term picture of strain imaged by geodesy.

Bell and others (2004) summarized all of the paleoseismic data for the CNSB, but little is known about the number and timing of prehistoric surface-rupturing earthquakes on the tens of Quaternary faults adjacent to the CNSB (for example, fig. 1). Many of these faults have geomorphic characteristics and neotectonic expressions that are similar to those faults that ruptured during historical earthquakes. The role that these various faults play in the long-term release of strain in west-central Nevada is unclear, and the interaction between adjacent faults is unknown. Could these adjacent faults be part of an expanding CNSB, or have they acted in concert with CNSB faults in prehistoric times? Has the late Quaternary strain release in the region been largely confined to

faults that ruptured historically or have nearby faults played significant roles? Studies to evaluate the paleoseismic history of the faults adjacent to the CNSB offer answers to some of these questions and increase our understanding of the spatial distribution of strain release over geologically significant time spans.

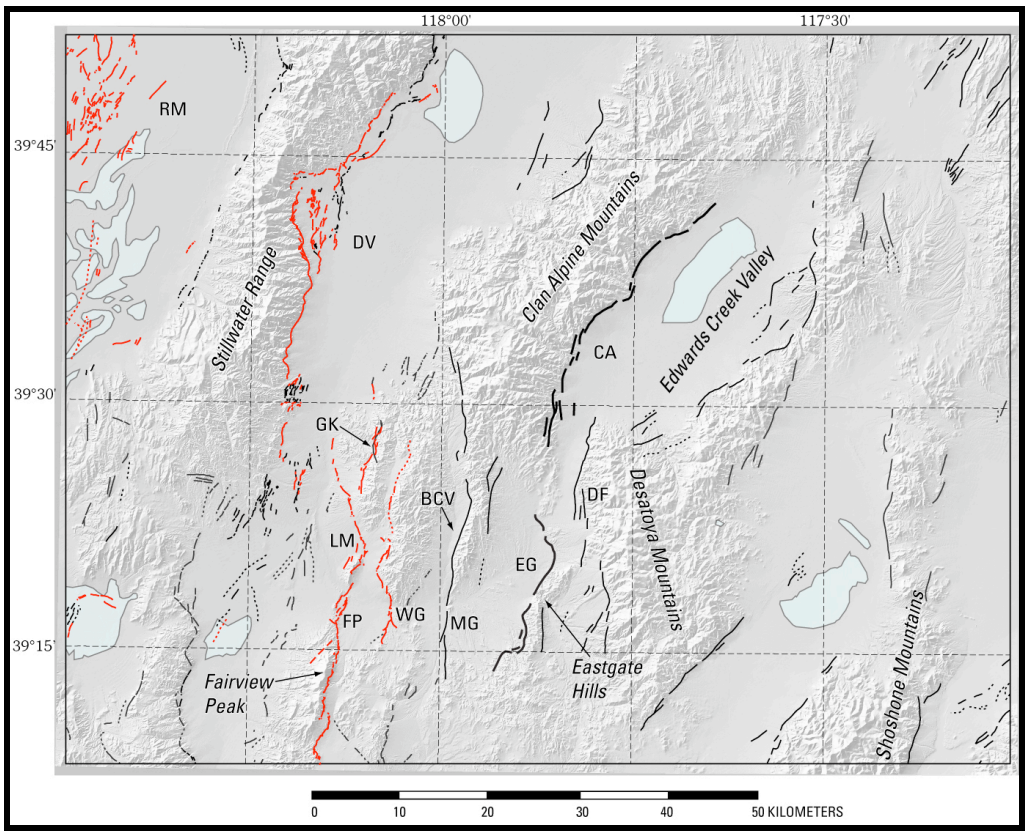

Figure 1. Shaded relief map of the Basin-and-Range province in west-central Nevada. Map is based on 30-m digital-elevation data (USGS) with illumination from the northwest. Historical surface ruptures from the 1954 Rainbow Mountain (RM), Dixie Valley (DV), and Fairview Peak (FP) earthquakes are shown as red lines; they include ruptures along the Westgate (WG), Louderback Mountain (LM), and Gold King (GK) faults. Heavy black lines show the surface traces of the Clan Alpine (CA) and Eastgate (EG) faults in the central part of the map area. Other Quaternary faults are shown by black lines; Desatoya fault (DF) and Middlegate fault (MG). Fault traces are from the USGS Quaternary fault and fold database available at: http://earthquake.usgs.gov/regional/qfaults/. BCV, Bench Creek Valley. Light gray areas in valleys are playa lakes.

Purpose

The Eastgate and Clan Alpine faults are located about 25–35 km east of the 1954 Fairview Peak and Dixie Valley surface ruptures in the CNSB. We studied the Eastgate and Clan Alpine faults 1) to determine if the CNSB faults have unique paleoseismic records or are more typical of a broader region that includes the Eastgate and Clan Alpine faults, 2) to help characterize specific Quaternary faults in north-central Nevada where GPS data show anomalous amounts of strain release patterns or high gradients in the strain field (Hammond and Thatcher, 2004), and 3) to determine the slip rates and recurrence intervals for two typical BRP extensional faults. By developing a paleoseismic record for these faults, we can compare a long-term late Quaternary geologic record with the

relatively short GPS signatures of strain release across the region. The age control for our studies relies primarily on luminescence and cosmogenic dating techniques rather than conventional radiocarbon dating because it is rare to find suitable organic material for radiocarbon dating in desert environments. By comparing the paleoseismic histories of these two faults with the histories of other faults in the CNSB, we can evaluate possible temporal interactions and patterns of late Quaternary strain release.

Seismologic Setting

The Eastgate and Clan Alpine faults are located 25–35 km east of Dixie Valley and Fairview Peak, where two major earthquakes in the CNSB produced about 100 km of surface rupture on December 16, 1954 (Caskey and others, 1996). In addition to ruptures on major range-bounding faults during these earthquakes, small-displacement, sympathetic surface ruptures formed along 8.5 km of the Gold King fault, 14 km of the Louderback fault, and 10 km of the Westgate fault, all of which are north and east of the Fairview Peak fault (Caskey and others, 1996). All of these faults dip to the west in contrast to the east-dipping Fairview Peak fault. The Middlegate fault, which forms the southwestern margin of the Clan Alpine Mountains, lies between the Westgate and Eastgate faults, and although poorly understood, it has a morphologically fresh appearance with steep scarps on bedrock. The Middlegate fault is a north-striking, narrow zone of relatively continuous faults that juxtapose bedrock of the Clan Alpine Mountains against Quaternary piedmont deposits of the Bench Creek Valley. The most recent surface rupture on this fault is thought to be late Quaternary in age (<130 ka) (USGS, 2006), but it could be Holocene. The Clan Alpine and Eastgate faults, along with the Desatoya fault (Koehler, this guidebook), which bounds the western side of the Desatoya Mountains, are three of the many faults in west-central Nevada that show evidence of late Pleistocene (10–130 ka) or Holocene (<10 ka) movement (Machette, 2005).

The historical seismicity in this part of western Nevada is dominated by aftershocks of the 1954 sequences (fig. 2), whereas in the area between the Clan Alpine and Desatoya Mountains, seismicity is scattered, diffuse, and cannot be clearly associated with the Clan Alpine, Eastgate, or Desatoya faults. Most of these earthquakes were small enough that probably they were not felt, but instead were located instrumentally with an epicentral accuracy of about 5–10 km. These data show no apparent spatial association between the M>3 earthquakes and traces of Quaternary faults in the study area with the exception of the down-dip extensions of faults that ruptured during the 1954 Fairview Peak and Dixie Valley earthquakes (that is, long-term aftershocks). Elsewhere in the study area, earthquake epicenters are distributed randomly among the basins and ranges. This lack of association between faults and earthquakes is similar to other parts of the intermountain west such as the Wasatch fault in Utah (Machette and others, 1992) and the Rio Grande rift in New Mexico (Machette, 1998).

Studies of the Clan Alpine and Eastgate Faults

Late Quaternary movement on the Eastgate and Clan Alpine faults has produced prominent scarps that are east and west, respectively, of U.S. Highway 50 (the “Loneliest Road In America”), which is a main east-west transportation route through the area (fig. 3). These two faults are roughly equidistant between Austin and Fallon, Nevada, in the west-central part of the Basin and Range province. Cold Springs Station, an isolated 1860s-era Pony Express waystation, is located along Highway 50 between these two north-striking faults.

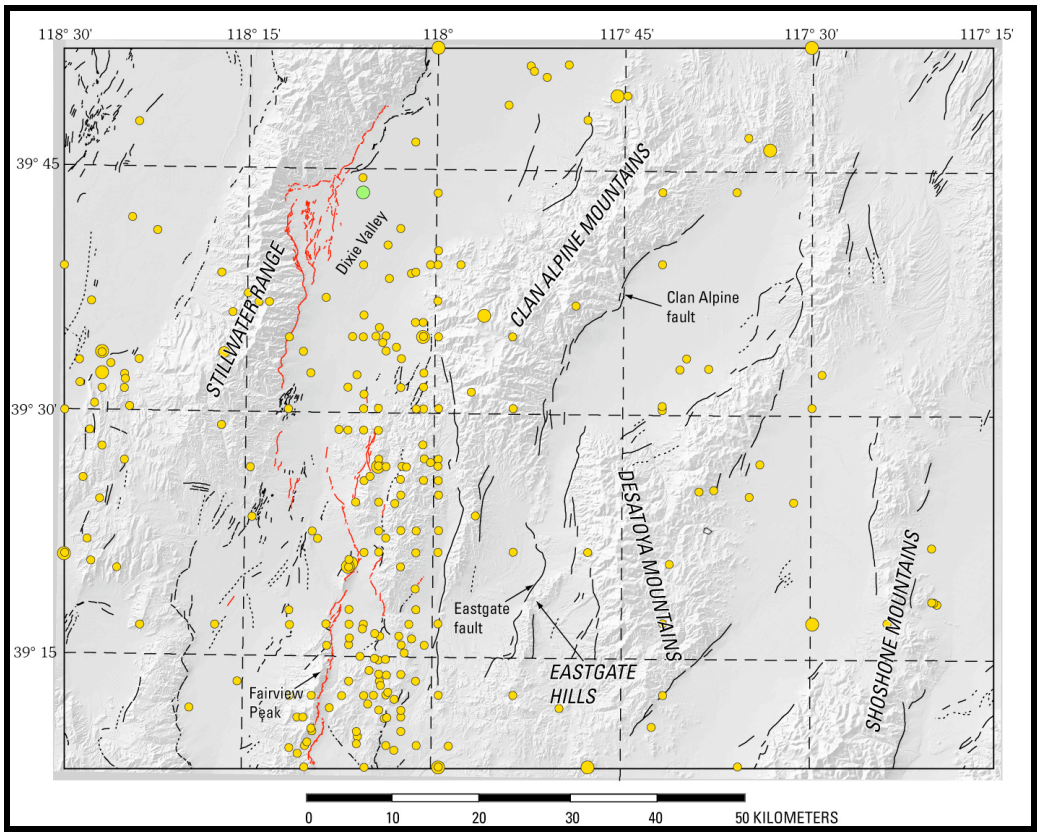

Figure 2. Seismicity of the Basin and Range province in west-central Nevada. Small dots show locations of 3>M>5 earthquakes, and large dots show locations of M>5 earthquakes reported between 1872 and 2005 in USGS catalogs. All earthquakes have depths of 33 km or less except for green dot, which has a depth of between 33–71 km. Quaternary faults are shown by black lines. Historic ruptures from the 1954 Dixie Valley and Fairview Peak earthquakes are shown in red, modified from Caskey and others, 1996. Fault traces are from the USGS Quaternary fault and fold database available at: http://earthquake.usgs.gov/regional/qfaults/. Seismicity plot courtesy of M. Zirbes, USGS.

The 33-km-long, east-dipping Clan Alpine fault bounds the eastern range front of the Clan Alpine Mountains and separates the range from the Edwards Creek Valley on the east, which was filled by pluvial Lake Edwards. The 18-km-long, west-dipping Eastgate fault is defined by a sinuous network of west-facing scarps that trend roughly northward from about 2 km south-southwest of the settlement of Eastgate, across U.S. Highway 50 south-southwest of Cold Springs Station, Nevada, to a prong of bedrock hills that extend south from the end of the Clan Alpine Mountains (fig. 3). The best geomorphic expression of the Eastgate fault in Quaternary deposits is only about 12 km long, but similar to the Clan Alpine fault, it has scarps of differing heights on Quaternary deposits of differing ages, indicating recurrent Quaternary movement. Scarps are more than 7 m high on Quaternary deposits that could be middle or early Pleistocene in age and are typically 1–2 m high on Holocene deposits.

At its northern and southern ends, the Eastgate fault juxtaposes Quaternary alluvium against early Miocene to Oligocene silicic volcanic rocks (Stewart and Carlson, 1978) that crop out in low bedrock hills. Along its central part, the fault is marked by prominent scarps that are on the distal parts of a broad alluvial piedmont that extends southwestward from the Desatoya Mountains.

Along its length, the fault scarp is dissected by drainage channels that are incised into the piedmont deposits, but between drainages, scarps are largely continuous and undissected.

Figure 3. Google Earth image of west-central Nevada showing the locations of trenches on the Eastgate and Clan Alpine faults. Historical surface ruptures from the 1954 Dixie Valley and Fairview Peak earthquakes are shown as red lines. The Eastgate fault is shown in orange as a Holocene fault. The Clan Alpine and other faults shown in green are late Pleistocene faults. Fault traces are from the USGS Quaternary fault and fold database available at: http://earthquake.usgs.gov/regional/qfaults/.

To evaluate the paleoseismic history of the Eastgate and Clan Alpine faults, we conducted photogeologic and field studies, including measuring the profiles of scarps on surficial deposits of middle(?) Pleistocene to Holocene age. We excavated two trenches on each fault at sites where we could best define a faulting history. However, our choice of potential sites was limited on both faults, but more so for the Clan Alpine fault because it is located mostly in the Bureau of Land Management's (BLM) Clan Alpine Wilderness Study Area (WSA), where the use of motor vehicles and machinery are currently prohibited. Similarly, the Eastgate fault crosses a small parcel of private property near Eastgate, but is mostly on BLM-controlled land. The basic field relations and detailed trench maps for each fault were published by Machette and others (2005) and Crone and others (2006).

We located our trenches where the faults offset a variety of Quaternary deposits and where faulting has juxtaposed fault-scarp colluvium against largely unconsolidated Quaternary deposits. In this type of setting, we had the potential to correlate deposits across the fault, which allows us to

measure the stratigraphic throw associated with individual surface ruptures. In all of our trenches, we mapped the north- or northwest-facing trench walls (because they remained out of direct sunlight for most of the day) using an electronic distance measuring (EDM) device to precisely locate points on trench walls. Detailed topographic profiles along the trench and companion profiles a few tens of meters on either side of the trench document the scarp's morphology at our sites (Machette and others, 2005; Crone and others, 2006).

On the Eastgate fault, our Central Eastgate site (CEG) is located where the 6.6-m-high scarp cuts an alluvial piedmont; this scarp has a maximum slope of 17.3° (fig. 4; about 120 m south of the field trip stop). The North Eastgate site (NEG) is located near the northern end of the fault, a few hundred meters north of U.S. Highway (fig. 4), where the 5.9-m-high scarp has a maximum slope angle of 15.6°. The size of these scarps is first-order evidence that they are the product of multiple surface-rupturing events, and the presence of 1- to 2-m-high scarps with steep slope angles (13°–15°) is morphological evidence that suggests the youngest event is probably middle Holocene in age (see profiles in Crone and others, 2006).

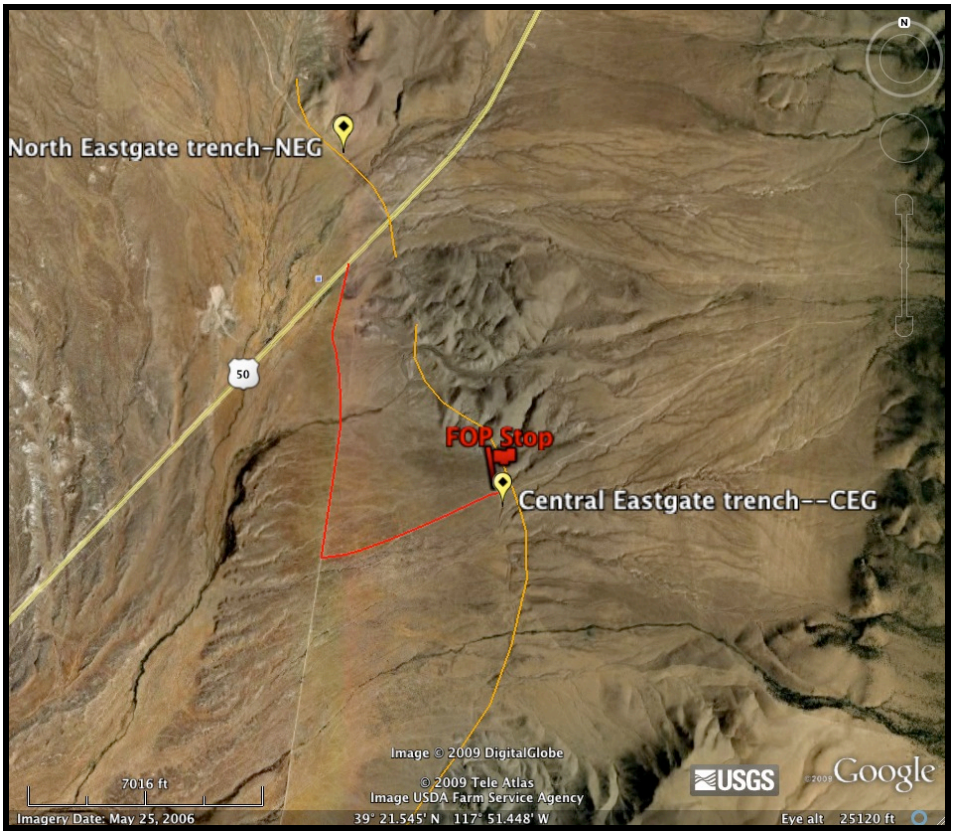

Figure 4. Google Earth image showing locations of the Central Eastgate and Northern Eastgate trenches. Red line shows the route from U.S. Highway 50 to the field trip stop. Orange line shows generalized trace of the Eastgate fault from the USGS Quaternary fold and fault database.

On the Clan Alpine fault, the Clan Alpine West (CAW) site is located near the southern end of the main western strand, where the scarp is 7.3 m high. The Clan Alpine East (CAE) site is located on a 2- to 3-m-high, uphill-facing, antithetic fault, which is about 1.2 km east of the main fault. On the eastern strand, the fault is partially buried by sediment that has accumulated against the scarp.

Summary of Paleoseismic History of the Eastgate Fault

We exposed evidence of four late Quaternary surface-faulting events in the CEG trench that resulted in displacement on three zones of faults (the main fault zone, a sympathetic mid-trench fault zone, and an antithetic fault zone), produced multiple colluvial wedges, and created a hanging-wall graben (fig. 5; see also Crone and others (2006) for detailed trench maps and related information). PE4, the oldest event, created a 14-m-wide graben that filled primarily with fine-grained eolian sediment. We estimate that PE4 produced a minimum of 1.1 m of vertical displacement and occurred about 31 ka based on stratigraphic relations and constraints from luminescence dates. Next, PE3 produced a well-defined colluvial wedge adjacent to the main fault zone. Based on the thickness of this wedge and compensating for a small amount of displacement on the antithetic fault zone, we estimate that about 1.9–2.0 m of vertical displacement occurred at this site on the Eastgate fault at about 25 ka. We estimate that 2.1–2.2 m of vertical offset occurred during the next younger earthquake, PE2, and our luminescence ages suggest a best-estimated age for this event of 18–20 ka. The youngest event, PE1, produced displacement mainly on the mid-trench fault zone. A small amount of displacement likely occurred on the main fault zone during PE1, but post-faulting erosion prevents measuring the exact amount. We estimate that about 1.3 m of net vertical displacement occurred during PE1, and although poorly constrained, our luminescence ages suggest that this event occurred about 5 ka.

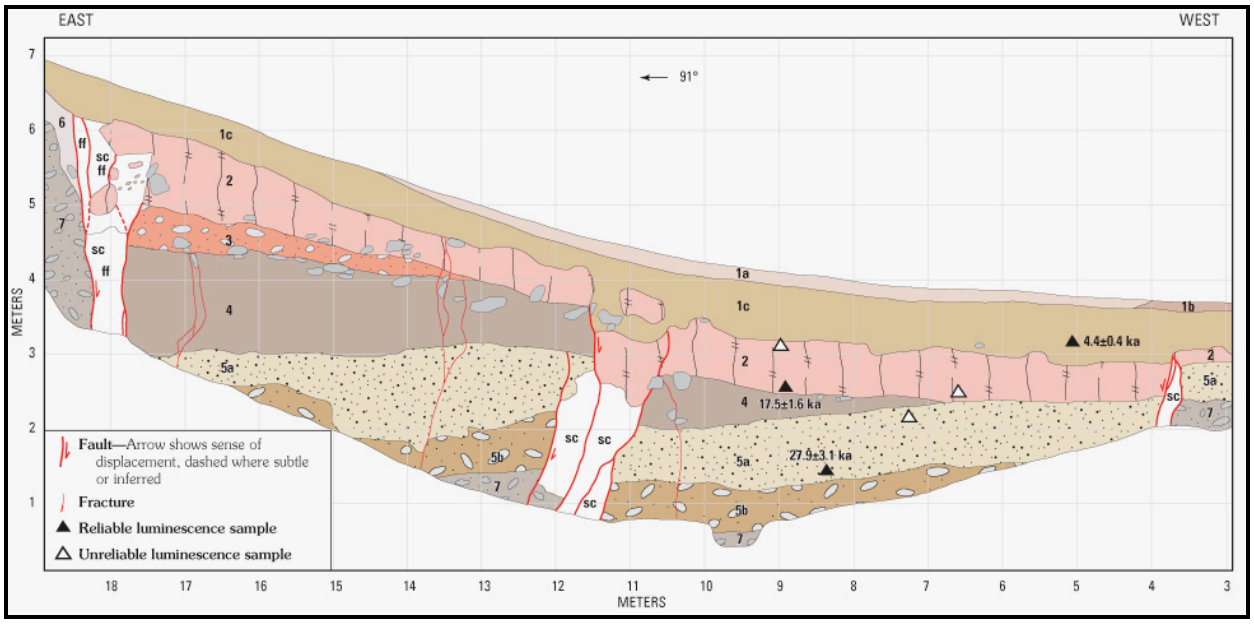

Figure 5. Schematic diagram of stratigraphic units and faults in the Central Eastgate (CEG) trench. The main fault zone near 18 m and the antithetic fault zone near 4 m define the edges of a graben. A mid-trench fault zone is present near 12 m. We collected and analyzed six luminescence samples from this trench but only those that have ages adjacent to the sample locations were deemed to yield reliable results; see Crone and others (2006) of details and for descriptions of units. Abbreviations: sc, sheared colluvium; ff, fissure fill.

In the NEG trench, colluvial deposits provide evidence of four surface-faulting earthquakes that produced more than 5.2 m of vertical displacement in the past 59 ka. The ages of all four of these events are poorly constrained but are younger than 59 ka, which is the age of fluvial or fluvio-lacustrine deposits in the footwall. PE4 can only be constrained to be younger than 59 ka, and based on the small amount of eolian silt in its colluvium, it may predate the major desiccation of

pluvial lakes in the region. The ages of events PE3 and PE2 are only constrained by the presence of weak to moderate calcic soil horizons (stage I to weak stage II) that formed on the colluvium from these two events. In climatic conditions typical of late Quaternary time in the region, these types of calcic soils require at least several thousand to possibly more than 10,000 years to form, so the inter-event times between PE2 and PE3 and between PE1 and PE2 are probably on the order of 5–10 ka. In the absence of any constraints on the age of PE1 at the NEG site, we infer that PE1 here could be contemporaneous with PE1 in the CEG site, that is, about 5 ka. This age is consistent with the scarp profile data (Crone and others, 2006).

Our preferred ages for events PE2 and PE3 are 18–20 ka and 25 ka, respectively, based on age constraints in the CEG trench, and our estimates of the net vertical displacement associated with these events are 2.1 and 1.9 m, respectively. Using these values, we calculate slip rates of about 0.12 and 0.20 mm/yr for the time intervals between events PE1 and PE2, and PE2 and PE3, respectively. If we use the entire time interval between events PE1 and PE3, the longer-term slip rate is about 0.15 mm/yr, which is our preferred rate for the Eastgate fault.

Summary of Paleoseismic History of the Clan Alpine Fault

In the CAW trench, we exposed direct and indirect evidence for a minimum of three, and probably four faulting events that have offset a piedmont alluvium that could be as old as middle Pleistocene in age (about 250 ka) (see Machette and others (2005) for detailed trench maps and related information). We mapped two colluvial wedges associated with the main fault that correspond to PE1 (Paleoearthquake 1), the most recent event, and PE2, the preceding surface-rupturing earthquake. PE1 and PE2 produced about 4 m of total throw across the fault zone. The PE1 and PE2 colluvial wedges are on a thicker wedge-like body of fluvial gravel and alluvial-fan deposits that we interpret to be slope colluvium and fluvial gravel that was deposited against the scarp formed by a prior third faulting event (PE3). The lowest unit on the hanging-wall block is a well-sorted, sandy pebble to boulder gravel that was deposited against a buried, preexisting fault scarp formed on the upthrown fault block.

Direct stratigraphic evidence of the older events in the form of colluvial wedges is not preserved in the trench, but stratigraphic relations indicate that one or more faulting events must have occurred between deposition of the PE2 colluvial wedge and the old piedmont deposits. The minimum cumulative throw on the piedmont alluvium is estimated to be at least 7–8 m, or roughly twice the throw estimated to result from events PE1 and PE2 (about 4 m of net throw). Thus, the 7.3-m-high scarp at the CAW site is likely the result of at least three and probably four discrete faulting events if the cumulative throw from the older events was comparable to the throw from events PE1 and PE2.

On the basis of OSL luminescence dates, PE1 likely occurred about 8.6–10 ka, and PE2 occurred about 30 ka, which is probably considerably younger than the underlying piedmont alluvium that they displaced. The age(s) of the older event(s) are unconstrained by the luminescence dating, but we anticipate that pending ^{36}Cl cosmogenic dates will determine the age of the faulted piedmont deposits and thus establish a maximum limiting age of faulting at this site.

In the CAW trench, we infer that there is a minimum of 7 m of vertical offset of deposits that we mapped as old Quaternary alluvium (Qao). This offset results from three or four events, which implies an average vertical offset of 1.7–2.3 m per event, and a recurrence interval of between 30 ky and 60 ky (3–4 events between about 10 ka and 130–250 ka, our estimated possible age range for

unit Qao). The only slip rate that we can calculate is between PE1 and PE2, which is 0.04–0.06 mm/yr (0.8–1.2 m offset in PE1 over a 20 ky time interval).

The CAE trench exposed antithetic faults, two colluvial wedges (units 1-2 and 2-2, fig. 7 in Machette and others, 2005), and a possible colluvial deposit (unit 3) that we interpret to be scarp colluvium and fluvial gravel that was deposited against a preexisting scarp from a third faulting event (PE3) of unknown offset.

We believe that ruptures on the antithetic fault at the CAE site correspond to major ruptures on the main fault because the antithetic displacements average more than 1.5 m per event. This suggests a direct link to the main fault zone at depth, rather than the antithetic fault having a small amount of sympathetic slip, such as occurred on adjacent faults during the 1954 Fairview Peak earthquake (Caskey and others, 1996).

Our luminescence ages suggest that PE1 produced surface rupture about 10 ka at the CAW and CAE sites. The time of PE2 is constrained by a minimum luminescence date of 27.6 ka, which we round upward to a general time of 30 ka. The ages of the older events, PE3 and PE4, remain unconstrained at present, although pending cosmogenic isotope dating (^{36}Cl) to determine the age of the faulted surfaces should define a maximum age for all events.

We expect that the formation of these piedmont surfaces is linked to late Quaternary climatic events and correlate with Oxygen Isotope Stage (OIS) IV (about 60–70 ka) or OIS VI (about 130–140 ka) although the Qao deposits could be older (OIS VIII?). Thus, the cumulative faulting of these surfaces places constraints on possible longer-term slip rates and recurrence intervals.

Our favored slip rate for the fault is on the order of 0.03–0.07 mm/yr, but this is largely based on the interevent time and displacement between PE1 and PE2. This value may change when we have a longer-term slip rate, but it is not likely to change by an order of magnitude. The fault's activity is best characterized as having a low slip rate and relatively long recurrence intervals (20 ky) as inferred from the time between the past two events and the longer-term average of perhaps four events in the last 130–250 ka.

Implications of Prehistoric Events on the Clan Alpine and Eastgate Faults

In table 1, we summarize our preferred ages for paleoearthquakes on the Clan Alpine and Eastgate faults. The correlation of prehistoric events between the two faults is poor, with only a possible correlation being Clan Alpine event PE2 (about 30 ka) perhaps correlating with Eastgate event PE4. The correlation of events PE1 on both faults is not likely, but not entirely impermissible given the poor age constraints for PE1 on the Eastgate fault. The absence of age constraints for Clan Alpine events PE3 and PE4 preclude correlating them with events on the Eastgate fault. Lastly, the 18–20 ka Eastgate PE2 and 25 ka Eastgate PE3 events do not appear to correspond to any Clan Alpine events.

Table 1. Summary of Preferred Ages of Prehistoric Earthquakes on the Clan Alpine and Eastgate Faults, Central Nevada. PE, paleoearthquake. Uncertainties in the estimated ages of individual events are large, so it is difficult to confidentially correlate events between the faults.

Fault Name	PE1	PE2	PE3	PE4
Clan Alpine	8.6–10 ka	~30 ka	<120–130 ka?	<120–130 ka?
Eastgate	~5 ka	18–20 ka	25 ka	31 ka/<59 ka

Given the proximity and orientation of the faults, one might expect a better correlation of events because they lie roughly on-end and along strike, and are only separated by a gap of about 8 km. Yet our studies suggest significantly different paleoseismic histories, inferring that the faults generally behave independently. One factor that likely contributes to this independent behavior is the opposing dips of the faults: the east-dipping Clan Alpine fault versus the west-dipping Eastgate fault. However, if Clan Alpine event PE2 does correlate with Eastgate event PE4, then some late Pleistocene events may have ruptured both faults.

In a regional context, the Eastgate fault would appear to be a minor seismic source because of its short length (12-18 km) and the lack of major topography associated with it. Major range-bounding faults, such as the Clan Alpine and Desatoya faults (fig. 3), would be viewed as the structures likely to accommodate most of the long-term regional extension. Interestingly, our studies suggest that the relatively short Eastgate fault has ruptured more frequently in the latest Pleistocene and has a higher slip rate than the nearby Clan Alpine fault.

Given its short length and absence of major associated topography, we speculate that the Eastgate fault may not always rupture as an independent seismic source, but at times may rupture in conjunction with earthquakes that originate on nearby major range-bounding faults. Our data suggest that Eastgate PE4 may be contemporaneous with Clan Alpine PE2, but other times, the Eastgate fault may rupture independently or possibly may rupture in conjunction with large earthquakes on the nearby Desatoya fault. Detailed ages of paleoevents on the Desatoya fault may clarify the interaction between these three neighboring faults.

References Cited

Bell, J.W., Caskey, S.J., Ramelli, A.R., and Guerrieri, Luca, 2004, Patterns and rates of faulting in the central Nevada seismic belt, and paleoseismic evidence for prior beltlike behavior: Bulletin of the Seismological Society of America, v. 94, no. 4, p. 1,229–1,254.

Bennett, R.A., Wernicke, B.P., and Davis, J.L., 1998, Continuous GPS measurements of contemporary deformation across the Basin and Range province: Geophysical Research Letters, v. 25, p. 563–566.

Bennett, R.A., Wernicke, B.P., Niemi, N.A., Friedrich, A.M., and Davis, J.L., 2003, Contemporary strain rates in the northern Basin and Range province from GPS data: Tectonics, v. 22, no. 2, p. 1,008, doi:10.1029/2001TC00355.

Caskey, S.J., Wesnousky, S.G., Zhang, Peizhen, and Slemmons, D.B., 1996, Surface faulting of the 1954 Fairview Peak (Ms 7.2) and Dixie Valley (Ms 6.8) earthquakes, central Nevada: Bulletin of the Seismological Society of America, v. 86, no. 3, p. 761–787.

Crone, A. J., Kyung, J.-B., Machette, M.N., Lidke, D,J., Okumura, Koji, and Mahan, S.A., 2006, Data related to late Quaternary surface faulting on the Eastgate fault, Churchill County, Nevada: U.S. Geological Survey Scientific Investigations Map SI 2893, 1 oversize plate [Available at: http://pubs.usgs.gov/sim/2005/2893].

de Polo, C.M., Clark, D.G., Slemmons, D.B., and Ramelli, A.R., 1991, Historical surface faulting in the Basin and Range province, western North America—Implications for fault segmentation: Journal of Structural Geology, v. 13, no. 2, p. 123–136.

Hammond, W.C., and Thatcher, Wayne, 2004, Contemporary tectonic deformation of the Basin and Range province, western United States: 10 years of observation with the Global Positioning System: Journal of Geophysical Research, v. 109**,** B08403, doi:10:1029/2003JB002746.

Machette, M.N., 1998, Contrasts between short- and long-term records of seismicity in the Rio Grande rift—Important implications for seismic-hazards analysis in areas of slow extension, *in* Lund, W.R., ed., Western States Seismic Policy Council (WSSPC) Proceeding Volume, Basin and Range Province Seismic-Hazards Summit: Utah Geological Survey Miscellaneous Publication 98-2, p. 84–95.

Machette, M.N., 2005, Summary of the late Quaternary tectonics of the Basin and Range province in Nevada, Eastern California, and Utah, *in* Lund, W.R., ed., Proceedings Volume, Basin and Range Province Seismic Hazards Summit II, Western States Seismic Policy Council, Reno, Nevada, May 16–91, 2004: Utah Geological and Mineral Survey Miscellaneous Publication 05-2.

Machette, M.N., Personius, S.F., and Nelson, A.R., 1992, The Wasatch Fault Zone, U.S.A., *in* R.C. Bucknam and P.L. Hancock, eds., A comparison of major active faults in diverse geologic settings: Special Issue of Annales Tectonicae (Dec. 1992), Supplement to v. 6, p. 5–39.

Machette, M.N., Haller, K.M., Ruleman, C.A., Mahan, S.A., and Okumura, Koji, 2005, Evidence for late Quaternary movement on the Clan Alpine fault, west-central Nevada–Trench logs, location maps, and sample and soil descriptions, U.S. Geological Survey Scientific Investigation Map SI–2891. [Available at: http://pubs.usgs.gov/sim/2005/2891]

Stewart, J.H., and Carlson, J.E., 1978, Geologic map of Nevada: U.S. Geological Survey, scale 1:500,000.

Thatcher, Wayne, Goulger, G.R., Julian, B.R., Svarc, J., Quilty, E., and Bawden, G.W., 1999, Present-day deformation across the Basin and Range province, western United States: Science, v. 283, p. 1,714–1,718.

U.S. Geological Survey (USGS), 2006, Quaternary fault and fold database of the United States, accessed August 14, 2009, http://earthquake.usgs.gov/regional/qfaults/.

Wallace, R.E., 1984, Patterns and timing of late Quaternary faulting in the Great Basin province and relation to some regional tectonic features: Journal of Geophysical Research, v. 89, no. B7, 5,763–5,769.

APPENDIX C

Diffusion Equation Representations of Landform Evolution in the Simplest Circumstances

Thomas C. Hanks
U.S. Geological Survey
Menlo Park, California 94025

Diffusion-Equation Representations of Landform Evolution in the Simplest Circumstances

Thomas C. Hanks
U.S. Geological Survey,
Menlo Park, California 94025

The *diffusion equation* is one of the three great partial differential equations of classical physics. It describes the flow or diffusion of heat in the presence of temperature gradients, fluid flow in porous media in the presence of pressure gradients, and the diffusion of molecules in the presence of chemical gradients. [The other two equations are the *wave equation*, which describes the propagation of electromagnetic waves (including light), acoustic (sound) waves, and elastic (seismic) waves radiated from earthquakes; and *LaPlace's equation*, which describes the behavior of electric, gravitational, and fluid potentials, all part of potential field theory. The diffusion equation reduces to LaPlace's equation at steady state, when the field of interest does not depend on *t*. *Poisson's equation* is LaPlace's equation with a source term.]

Joseph Fourier developed the diffusion equation for heat conduction in 1807, and it has significant associations with probability theory (Narasimhan, 2009), as we will see shortly. In a novel and fascinating application, Gene Humphreys has employed solutions of the diffusion equation to describe the density of desert tortoises in the presence of population gradients caused by new dirt roads cut in the Mojave Desert. These new dirt roads induce an immediate line sink for unsuspecting tortoises. As of this writing in early September, I am not sure whether Gene has published this work.

Most of us here know that the diffusion equation has also been used to describe the evolution through time of scarp-like landforms, including fault scarps, shoreline scarps, or a set of marine terraces. The methods, models, and data employed in such studies have been described in the literature many times over the past 25 years. For most situations, everything you will ever need (or want) to know can be found in Hanks *et al*. (1984) and Hanks (2000), the latter being a review of numerous studies of the 1980s and 1990s and a summary of available estimates of the mass diffusivity κ. The geometric parameterization of scarp-like landforms is shown in Figure 1.

The homogeneous diffusion equation with constant coefficients is

$$\partial u / \partial t - \kappa \partial^2 u / \partial x^2 = 0. \qquad (1)$$

In the case of landform evolution, u is relative elevation along the profile distance x, t is time, and $\partial u/\partial t$ is the rate of change of elevation with time. κ is the mass diffusivity and $\partial^2 u/\partial x^2$, the second spatial derivative of u, is the profile curvature. Equation (1) says that the rate of change of the profile elevation at some place x along the profile depends on its curvature at x. If the curvature is negative (convex up), elevation decreases (erodes) as

the profile sheds mass to lower elevations; this mass re-accumulates where the curvature is concave up (sedimentary basins) and elevation increases.

The solution to (1) for a step of topography $2a$ imposed at $x = 0$ and $t = 0$ upon a pre-existing surface of slope b (a single episode of vertical, dip-slip faulting of a fan surface with slope b) is

$$u(x,t) = a * erf\left(x / 2\sqrt{\kappa t}\right) + bx, \tag{2}$$

where *erf (ξ)* is the error function of argument ξ to which we will return. Equation (2) allows us to calculate elevation profiles directly.

One can also estimate the age of a scarp from its slope, or first spatial derivative. The maximum scarp slope occurs at $x = 0$, but we (Hanks and Andrews, 1989) have found it important to work with the *reduced scarp slope*, $\partial u/\partial x|_{x=0} - b$, to account for variable far-field slopes that arise in moving from one fan surface to another:

$$\partial u / \partial x \,|_{x=0} - b = a / \sqrt{\pi \kappa t}\,. \tag{3}$$

Measuring the scarp slope, the far-field slope, and scarp offset $2a$ are easy to do in the field, even with antique measuring devices. But we also need to know how error functions work.

Yes, it is true that

$$erf(\xi) = 2/\sqrt{\pi} \int_0^{\xi} e^{-\eta^2} d\eta, \tag{4}$$

but don't get hung up on the mathematical formalism here. We can look up the values of *erf (ξ)* for any ξ in books, at least "books" that have tables of mathematical functions. Values of *erf (ξ)* for some selected values of ξ are given in the table below, and *erf (ξ)* is shown graphically along with its kernel $e^{-\eta^2}$ in Figure 2.

ξ	erf (ξ)
0	0
0.1	0.125
0.2	0.223
0.3	0.329
0.4	0.428
0.5	0.521
0.6	0.604
0.7	0.678
0.8	0.742
0.9	0.797

1.0	0.843
1.1	0.880
1.2	0.910
1.5	0.966
2.0	0.995

Equation (4) looks a lot like the cumulative probability function that attends the normal (Gaussian) distribution function with mean value of 0, but there are some important differences. Cumulative probability functions are always positive, ranging from 0 and low probabilities to high probabilities and 1. The function *erf (ξ)* is anti-symmetric about $\xi = 0$; that is *erf (ξ)* = - *erf (-ξ)*. So the table above is twice as good as it looks. For $0 < \xi < |0.5|$, *erf (ξ)* is nearly linear, with a slope of ~1. The error function then rolls over to progressively lower slopes to attain its asymptotic values of ±1 (Figure 2).

The anti-symmetry of the error function is also important geologically, for it permits analysis of those landforms for which only half the scarp is preserved. For example, a fluvial terrace riser showing erosional degradation of its upper half may lack this detritus on its lower half if this detritus has been swept away by more recent flooding. Hanks and Schwartz (1987) demonstrated how the age of the earthquake preceding the Borah Peak earthquake (28 October, 1983; **M** = 7.0) could be obtained solely from the degraded scarp on the footwall block, the lower (hanging wall) part of this scarp having been faulted downward and partially covered by detritus from the free face of the 1983 scarp.

Yet another quick way to estimate the age of a scarp is to note that because *erf (y)* = 0.84 when $y = 1$, one can quickly estimate the value of $\left(x/2\sqrt{\kappa t}\right) = 1$ if one can accurately identify the scarp mid-height and where the scarp attains 84% of its full amplitude $2a$; x_{84} is the distance between them which allows for a quick calculation of $\kappa t = (x_{84}/2)^2$. Figure 2 shows x_{84} graphically. Figure 3a shows evaluations of equation (1) for $a = 1$m and $b = 0$ for various values of κt, and t for $\kappa = 1\text{m}^2/\text{ka}$, and Figure 3b shows evaluations of equation (2) for the same circumstances

Rich K tells me that we will be stopping in Grass Valley (Nevada) to see some fault and shoreline scarps, so we will try out some of these tricks, if anyone remembers to bring a measuring tape, straight edge, and Abney level.

Speaking of remembering stuff, the diffusion-equation modeling can only determine the product κt (*diffusion age*) from fitting models to data. To get an actual age for some single-event fault scarp, for example, one has to know separately the appropriate κ. In the Basin and Range province where we are now, κ is known from shorelines scarps of Lakes Bonneville and Lahontan. Remarkably, it is the same for both ($\kappa = 1\ \text{m}^2/\text{ka}$) when the effects of differing a and b among profiles are accounted for (Hanks and Wallace, 1985; Hanks and Andrews, 1989).

Note in Figure 3b that a 2m-high scarp (a = 1m) will ravel to ~30° (or about the angle of repose) in κt = 1 m^2 even for linear diffusion (for non-linear diffusion this will happen even faster). For κ = 1 m^2/ka, the free faces of $2a$ = 2m scarps should vanish in ~1000 years or less. What this means, if true, is that the initial geometry of small scarps does not make much difference, because it vanishes so quickly. Given the number of historic scarps in the Basin and Range province and what is known about young but still pre-historic scarps, this could and should be verified, but to my knowledge no one has done this yet.

Finally, while the product κt is often, but certainly not always well determined by profile data, κ may vary considerably as a function of climate, lithology, and vegetative cover. Moreover, one should expect quite generally that *erosional diffusivity*, what happens on the convex-up side, to be quite different from the *depositional diffusivity*, what happens on the concave-up side. So studies of the sort described above are only going to work in weakly consolidated terrains where these two diffusivities have a chance of being comparable. What was known a dozen years ago about diffusivities in weakly consolidated terrains is summarized in Hanks (2000). Spatially inhomogeneous diffusivities can be dealt with, but mostly through numerical solutions, also required for dealing with multiple fault scarps and the important matter of non-linear, down-slope transport.

References

(The references below are by no means complete, just easy for me to find.)

Bucknam, R.C. and Anderson, R.E. 1979, Estimation of fault-scarp ages from a scarp-height-slope-angle relationship, *Geology,* v. 7, 11-14.

Hanks, T.C., 2000, The age of scarplike landforms from diffusion-equation analysis, in Quaternary Geochronology Methods and Applications, J.S. Noller, J.M. Sowers, and W.R. Lettis, eds: *American Geophysical Union*, Washington, DC.

Hanks, T.C., and Andrews, D.J., 1989, Effect of far-field slope on morphologic dating of scarplike landforms: *Journal of Geophysical Research, v*. 94, p. 565-573.

Hanks, T.C, Bucknam, R.C., Lajoie, K.R., and Wallace, R.E., 1984, Modification of wave-cut and faulting-controlled landforms: *Journal of Geophysical Research,* v. 89, p. 5771-5790.

Hanks, T.C., and Schwartz, D.P., 1987, Morphologic dating of the pre-1983 fault scarp on the Lost River fault at Doublespring Pass Road, Custer County, Idaho: *Seismological Society of America Bulletin,* v. 77, p. 837-846.

Hanks, T.C., and Wallace, R.E., 1985, Morphological analyses of the Lake Lahontan shoreline and Beachfront fault scarps, Pershing County, Nevada: *Seismological Society of America Bulletin,* v. 75, p. 835-846.

Narasimhan, T.N. 2009. The dichotomous behavior of diffusion, *Physics Today*, v. 62, p. 48-53.

Figure Captions

1. Parameterization of a scarp profile, from Figure 1 of Hanks *et al*. (1984), itself mostly after Bucknam and Anderson (1979). In the terminology here b= tan θ_f and $\partial u/\partial x|_{x=0}$ = tan θ_s . H is the scarp amplitude measure of Bucknam and Anderson (1979), which depends on θ_f ; the scarp offset $2a$ does not.

2. The functions $erf(\xi)$ and $e^{-\eta^2}$.

3. (a) Evaluations of equation (1) and (b) equation (2) for a =1m and b = 0.

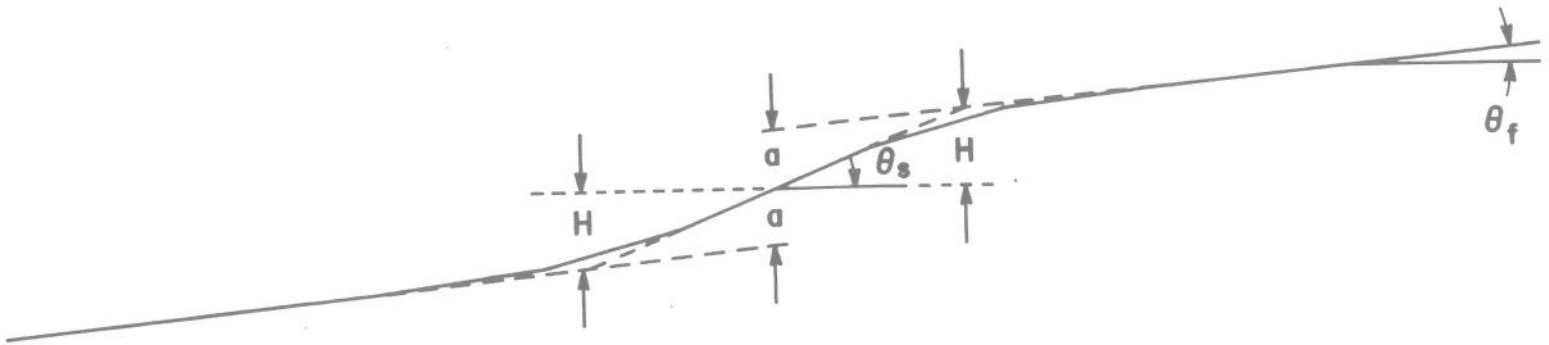

Fig. 1

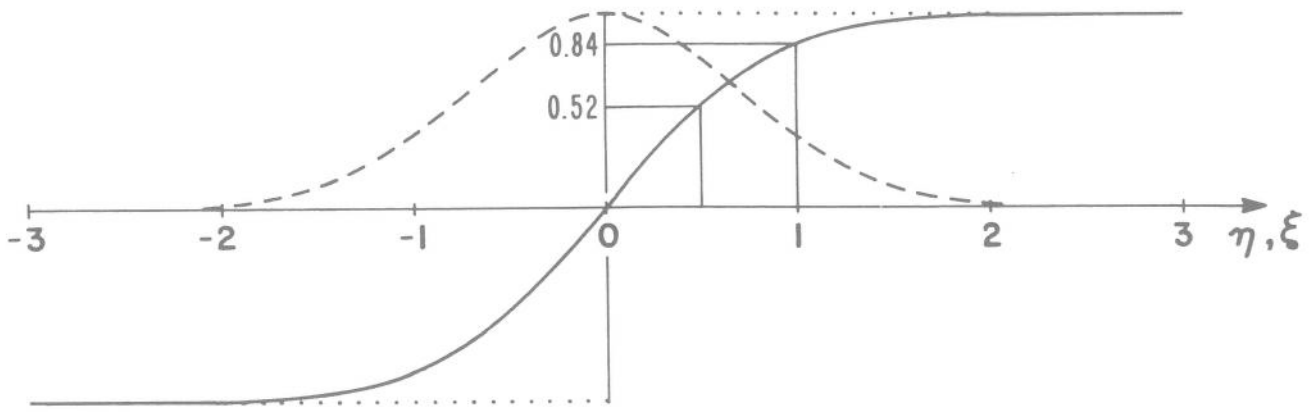

Fig. 2

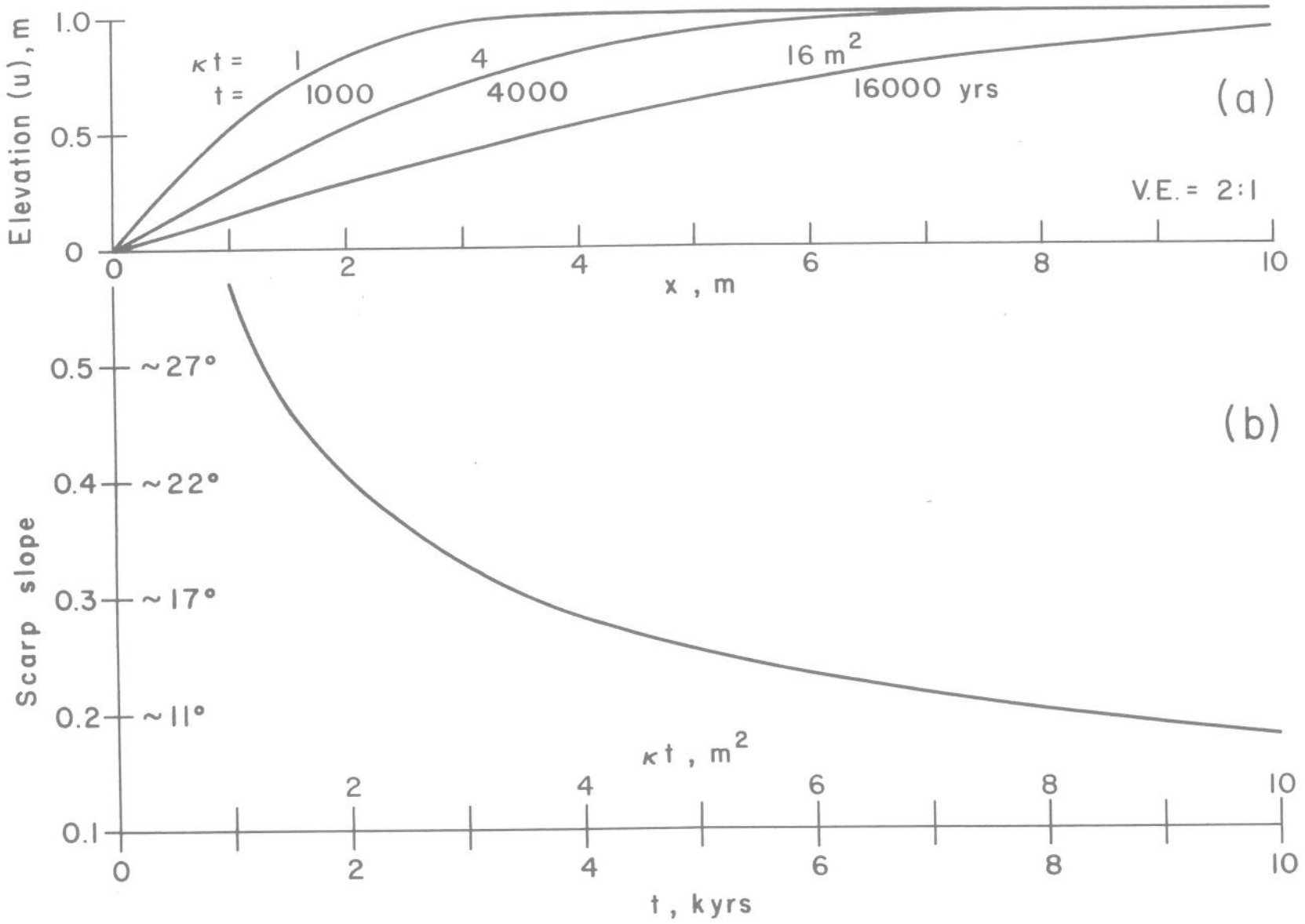
Elevation (u), m
1.0
0.5
0
κt = 1
t = 1000
4
4000
16 m²
16000 yrs
(a)
V.E. = 2:1
0
2
4
6
8
10
x , m
0.5
~27°
0.4
~22°
0.3
~17°
0.2
~11°
0.1
Scarp slope
(b)
κt , m²
2
4
6
8
10
0
2
4
6
8
10
t , kyrs

Fig. 3

APPENDIX D

Geodetic Constraints on Active Deformation of the Eastern Nevada Basin and Range Near Highway 50

William C. Hammond
Nevada Geodetic Laboratory
Nevada Bureau of Mines and Geology

Geodetic Constraints on Active Deformation of the Eastern Nevada Basin and Range Near Highway 50

William C. Hammond

for the Friends of the Pleistocene Field Trip Guide

Abstract

Geodetic studies estimate the patterns, rates and styles of crustal strain accumulation that complement neoteconic studies of past strain release. In the central part of the Basin and Range Province, several earlier geodetic studies found that deformation rates were not significantly greater than zero. More recent studies, stimulated by the occurrence of the 2008 Wells, Nevada earthquake have found that there is ~1 mm/yr of transtensional deformation over 300 km of eastern Nevada. This increase in precision has been made possible by utilizing long and stable GPS time series of the EarthScope Plate Boundary Observatory (PBO), and special analysis procedures that are devised specifically to isolate horizontal strain signals. The style and rate of this deformation is consistent with the extensional direction of the Wells earthquake, with the predominantly N-NNE strike of normal faults in the Great Basin, and with the prevailing pattern of dextral shear associated with Pacific/North America plate boundary deformation. The rate of deformation is also consistent, to within uncertainties, with the ~0.8 mm/yr of late Pleistocene extension found in the recently completed paleoseismic transect across ranges near Highway 50 [*Koehler and Wesnousky*, 2009].

Background

Geodetic studies complement neotectonic studies of active crustal deformation. Generally geologic studies focus on the slip activity of faults over 10^2 to 10^6 years at specific sites, while geodetic studies measure the rate of surface deformation over ~3-20 years. Geodetic and geologic studies have been shown to be in good agreement across the scale of major plates (with some caveats [e.g. *deMets et al.*, 1994]),and across many important plate boundary faults [*Thatcher,* 2009]. How well this agreement extends into smaller zones of distributed complex deformation, on regional to individual fault scales such as in the Basin and Range and Walker Lane is a topic of ongoing research. Close agreements between these very different types of measurements would suggest that 1) patterns and rates of strain accumulation (measured by GPS) match patterns of strain release (measured in fault studies) 2) that geodynamic processes responsible for observed faulting are presently active and measurable, and 3) that geodetic measurements can provide constraint on the potential for future earthquakes, and hence are an important tool for studies of seismic hazard.

In the past decade great progress has been made in understanding Pacific/North American plate boundary deformation patterns, rates and styles, which facilitates more accurate comparisons to geologic fault slip rates. In particular, across the Basin and Range near the latitude of Highway 50 rates have been estimated using GPS in several studies [e.g. *Thatcher et al.*, 1999; *Dixon et al.*, 2000; *Wernicke et al*, 2000; *Oldow et al*, 2001; *Bennett et al.*, 2003; *Hammond and Thatcher,* 2004]. These indicated that the North American plate 1) is to within measurement uncertainty rigid east of central Utah, 2) has a zone of 3-4 mm/yr of east-west extension across the easternmost Basin and Range near the Wasatch Fault, 3) has a zone of ~10 mm/yr of relative motion between the Basin and Range in central Nevada and the Sierra Nevada/Great Valley microplate (Figure 1). Several of these earlier studies concluded that the the rate of deformation across eastern Nevada, between the Wasatch and

the Walker Lane Belt, was not significantly different than zero, and thus was described as a "geodetic microplate", since it apparently moved as a rigid body westward with respect to stable North America.

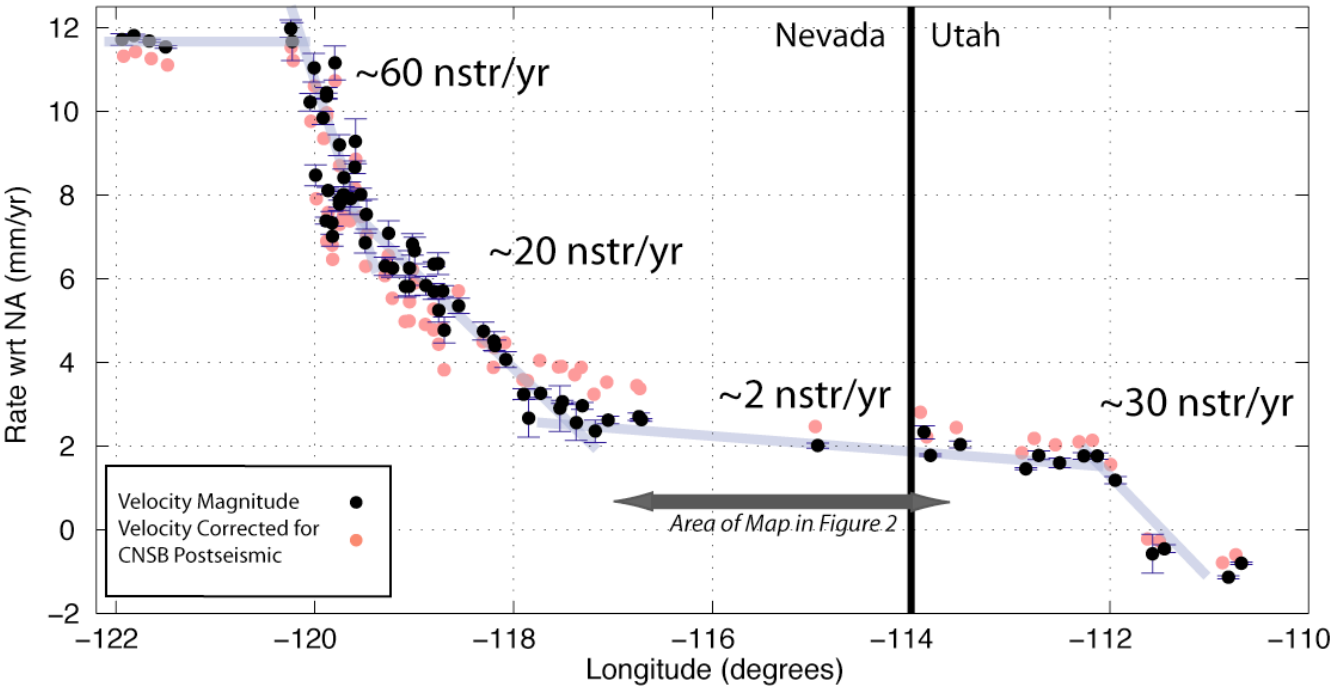

Figure 1. Magnitude of GPS velocity across Basin and Range Province between 39˚ and 40˚ north latitude (black dots) with respect to stable North America [SNARF, *Blewitt et al.*, 2005]. Variation of deforamtion is indicated by approximate scalar uniaxial strain rates indicated by slope of gray lines, at various intervals of longitude across the Province. Central Nevada Seismic Belt historic earthquakes likely contribute a transient velocity to these gradients. Subtracting a model for these transient effects [*Hammond et al.*, 2009a] perturbs these strain rates slightly (red dots).

Wells, Nevada, 2008 Earthquake

In February, 2008 the M_W 6.0 earthquake struck Wells, Nevada, inside the region generally thought to exhibit very low rates of crustal deformation. This prompted our study of the GPS data obtained from continuously recording sites nearest the epicenter to estimate coseismic displacements and secular trends in motion for the decade preceding the event [*Hammond et al.*, 2009b]). Since the most recent of the above cited studies were published, these GPS sites of the BARGEN (now EarthScope PBO) network (Figure 2) have recorded data for 5 additional years. The new data provide longer time series that improve the resolution of GPS velocity with respect to other sites in the network, so it is now possible to distinguish strain from velocity gradients associated with the rotation of a rigid central Nevada block. See example time series in Figure 3.

The velocity gradients are small, but consistent with approximately 1 mm/yr of deformation across the eastern Nevada Basin and Range. This velocity gradient is partially visible in the magnitude of velocity changes seen in Figure 1 between longitude -118˚ and -114˚ longitude. Using these velocities to solve for horizontal tensor strain rates and rotation parameters simultaneously indicates that 4.6±0.8 nanostrains year^{-1} of extension directed N59˚W, and 2.8±1.1 nanostrains year^{-1} contraction directed N31˚E occurred over the eight years of observation. In other words, the results indicate that after subtracting the effects of block rotation from the velocity estimates, a residual signal exists that can be attributable to deformation of the eastern Nevada Basin and Range (see magenta vectors in Figure 2).

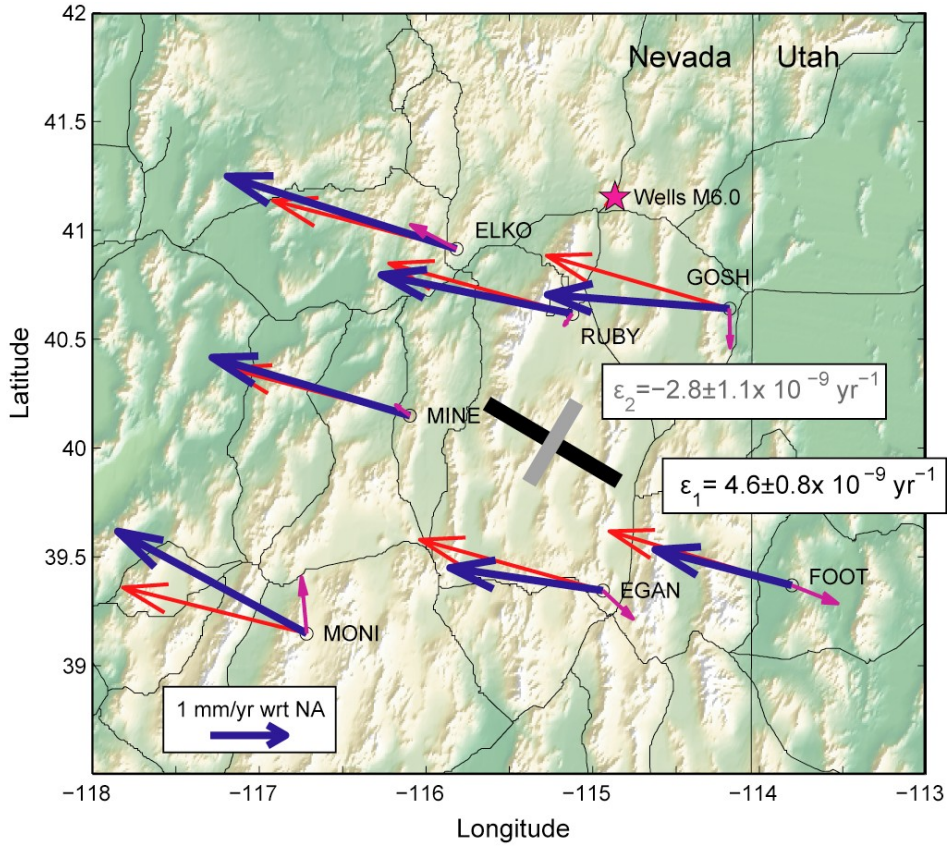

Figure 2. Background secular velocities with respect to stable North America of BARGEN/PBO permanent GPS sites preceding the Wells, NV earthquake (blue). Velocities attributable to deformation (magenta) have been inferred by subtracting the best fitting model of rigid rotation for these sites (red). This network is approximately 250 km wide and experiences about 7 nanostrains/yr of transtensional deformation. The maximum horizontal extension has azimuth N59˚W (black tensor strain rate bar), and maximum horizontal contraction has azimuth N31˚E (gray tensor strain rate bar). Location of Wells earthquake is shown with magenta star.

This estimate of crustal strain contributes to a well-integrated picture of the seismic cycle and crustal deformation of eastern Nevada that is consistent with seismic and geologic data. For example, the azimuth of the direction of maximum horizontal crustal extension as measured by GPS is very similar to the azimuth of coseismic extension that occurred during the Wells earthquake (T-axis N60˚W, Harvard CMT, www.globalcmt.org). This suggests that the long-term preseismic strain accumulation determined by GPS represents loading of the crust in preparation for the earthquake. Furthermore, the orientation of the GPS-measured shear in the crust is aligned with the predominant direction of shear that is prevalent in the western Basin and Range, and San Andreas fault system (Figure 3) and is consistent with this part of the Basin and Range behaving as an active component of the Pacific North/America plate boundary system. However, the N59˚W extension rate is approximately twice as large as the N31˚E contraction rate, indicating the state of deformation is transtensional, and possibly closer to uniaxial extension if the contraction rate is not significant.

The study of *Koehler and Wesnousky* [2009] provides a late Pleistocene rate of extension across the range bounding faults of eastern NV near Highway 50 of 0.8-1.0 mm/yr between the Toiyabe range and the NV/UT border. Thus the geologic estimate and geodetic estimate are in agreement to within the uncertainty of the measurements.

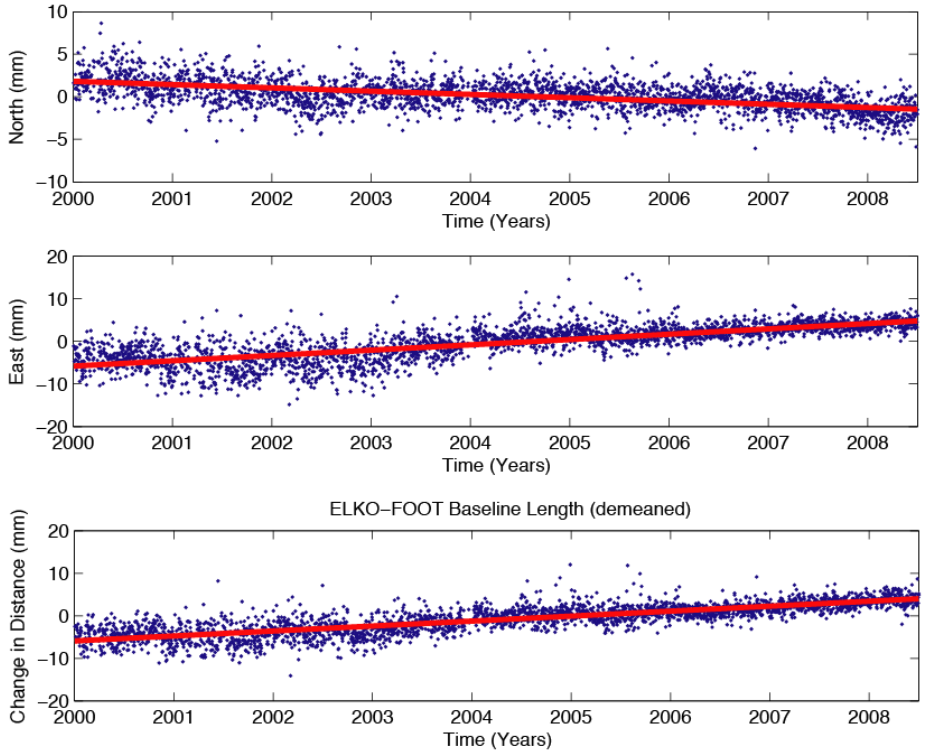

Figure 3. Example GPS time series showing trend of North (top) and East (center) coordinates of site ELKO with respect to site FOOT, and the distance between these sites (bottom). Data indicate that the distance between the sites steadily increased by ~10 mm between year 2000 and 2008. Line length changes require deformation and are not attributable to block rotation.

Central Nevada Seismic Belt Postseismic Relaxation

Following large earthquakes the lower crust and/or upper mantle can experience transient stress relaxation which can be detected with geodetic measurements. Several earthquake events occurred in Nevada during the past century that could potentially give rise to viscoelastic response. Since these signals are transient (i.e. decay to zero over years to decades) they should be accounted for when using geodesy to make estimates of long term crustal deformation patters. In this case we wished to investigate whether the strain we measured in eastern Nevada could be affected by postseismic relaxation from the 1954 Dixie Valley (M_W 6.9), 1954 Fairview Peak (M_W 7.0), 1915 Pleasant Valley (M_W 7.4), or the 1932 Cedar Mountain (M_W 7.1) events. These earthquakes, collectively referred to as the Central Nevada Seismic Belt (CNSB), were modeled in an earlier study [*Hammond et al.,*2009a]. We used this model to correct for the transient affects in the velocity profile (Figure 1). The results of the modeling indicate that transient motions could be detected in eastern NV, but they predict a sense of shear that is opposite to what is observed. However, uncertainties in the viscosity structure and rheology make the estimate of the very small transient uncertain at large distances and times from the earthquakes. Other similar models might predict slightly different patterns and rates of the transient, though they would likely not increase its contribution to above 1 mm/yr deformation across eastern NV.

The MAGNET GPS Network

The Mobile Array of GPS for Nevada Transtension (MAGNET) is a complement to the EarthScope PBO continuous network that densifies observations to ~20 km spacing (and sometimes more dense) in the western part of the Basin and Range and Walker Lane. The distribution of sites, and information about the network, can be found at http://geodesy.unr.edu/networks. This network has been established for research in GPS measurement of crustal deformation, and targeting of geothermal systems. Increasingly,

GPS measurements are used in the quantification of seismic hazard, and these data are in the process of being explicitly incorporated into the USGS Probabilistic Seismic Hazard Maps via block models, and crustal strain maps. The immediate future of our GPS monitoring will include 1) increasing geographic coverage of the networks to include other areas of tectonic interest, 2) obtaining longer time series on every site to enable more precise estimates of deformation (such as outlined in this study), and 3) combination of GPS with other complementary technologies, such as Interferometric Synthetic Aperture Radar (InSAR), to improve spatial resolution of monitoring. Each of these steps will continue the improvements in measuring Basin and Range crustal deformation that have been made over the last several decades.

Acknowledgements

Research that contributed to this work was supported by the National Science Foundation under grants 0610031 and 0635757, and by USGS support for the study of the 2008 Wells, Nevada earthquake. Data used in this study were obtained from the UNAVCO, Inc. archives.

References

Bennett, R. A., B. P. Wernicke, N. A. Niemi, A. M. Friedrich, and J. L. Davis (2003), Contemporary strain rates in the northern Basin and Range province from GPS data, *Tectonics*, *22, 1008, doi:10.1029/2001TC001355*.

Blewitt, G., D. F. Argus, R. A. Bennett, Y. Bock, E. Calais, M. Craymer, J. L. Davis, T. H. Dixon, J. T. Freymueller, T. A. Herring, D. Johnson, K. M. Larson, E. L. Miller, G. F. Sella, R. A. Snay, and M. Tamissiea (2005), A stable North America reference frame (SNARF): First release, paper presented at UNAVCO-IRIS Joint Workshop, Stevenson, Washington, June 8-11, 2005.

DeMets, C., R. G. Gordon, D. F. Argus, and S. Stein (1994), Effect of recent revisions to the geomagnetic reversal time-scale on estimates of current plate motions, *Geophysical Research Letters*, *21*, 2191-2194.

Dixon, T. H., M. Miller, F. Farina, H. Wang, and D. Johnson (2000), Present-day motion of the Sierra Nevada block and some tectonic implications for the Basin and Range province, North American Cordillera, *Tectonics*, *19*, 1-24.

Hammond, W. C., and W. Thatcher (2004), Contemporary tectonic deformation of the Basin and Range province, western United States: 10 years of observation with the Global Positioning System, *Journal of Geophysical Research*, *109, B08403, doi:10.1029/2003JB002746*.

Hammond, W.C., Kreemer, C., and Blewitt, G., 2009, Geodetic constraints on contemporary deformation in the northern Walker Lane: 3. Central Nevada seismic belt postseismic relaxation, in Oldow, J.S., and Cashman, P.H., eds., Late Cenozoic Structure and Evolution of the Great Basin–Sierra Nevada Transition: Geological Society of America Special Paper 447, p. 33–54, doi: 10.1130/2009.2447(03).

Hammond, W.C., G. Blewitt, C. Kreemer,J. R. Murray-Moraleda, J. L. Svarc, 2009, GPS constraints on crustal deformation before and during the 21 February 2008 Wells, Nevada M 6.0 Earthquake, NBMG/USGS 2008 Wells, Nevada Earthquake Report, in review.

Koehler, R., and S. G. Wesnousky (2009), Late Pleistocene regional extension rate derived from earthquake geology of late Quaternary faults across Great Basin, Nevada between 38.5 and 40 N latitude, *Geological Society of America Bulletin*, *in review*.

Oldow, J. S., C. L. V. Aiken, J. L. Hare, J. F. Ferguson, and R. F. Hardyman (2001), Active displacement transfer and differential block motion within the central Walker Lane, western Great Basin, *Geology*, *29*, 19-22.

Thatcher, W., 2009, How the continents deform: The evidence from tectonic geodesy, *Annu. Rev. Earth Planet. Sci.,* 37:237–62, doi:10.1146/annurev.earth.031208.100035.

Wernicke, B. P., A. M. Friedrich, N. A. Niemi, R. A. Bennett, and J. L. Davis (2000), Dynamics of plate boundary fault systems from Basin and Range Geodetic Network (BARGEN) and Geologic Data, *GSA Today*, *10*, 1-7.